J Solid State Electrochem (2011) 15:623–633
DOI 10.1007/s10008-010-1169-7

ORIGINAL PAPER

Structural and electrocatalytic features of Pt/C catalysts fabricated in supercritical carbon dioxide

Ernest E. Said-Galiyev · Alexander Yu. Nikolaev · Eduard E. Levin · Ekaterina K. Lavrentyeva · Marat O. Gallyamov · Sergei N. Polyakov · Galina A. Tsirlina · Oleg A. Petrii · Alexey R. Khokhlov

Received: 6 July 2010 / Revised: 3 August 2010 / Accepted: 5 August 2010 / Published online: 29 August 2010

Abstract Pt/carbon black samples fabricated from dimethyl (1,5-cyclooctadiene) platinum(II) in supercritical CO_2 are characterized in relation to possible applications in methanol fuel cell. The problem of precise material characterization is addressed in frames of X-ray diffractometry, transmission electron microscopy, and electrochemical techniques of the true surface area determination. The catalysts with Pt loading of 20–40 wt.% consist of nm-size particles, with the lattice defectiveness dependent on the fabrication mode. To check the effect of support, various types of carbon blacks (Vulcan XC72R and acetylene black AC-1) are used. In contrast to commercial HiSpec catalysts, no pronounced increase of particle size with Pt loading is found. Specific steady-state activity towards methanol oxidation appears to be essentially higher than for commercial catalysts, mostly because the self-poisoning effects are less pronounced. As for poisoning of Pt with organic species (resulting from the ligand of precursor), its effects are demonstrated to be minor after CO or methanol adsorption accompanied by desorption of contaminating by-product.

Keywords Supercritical carbon dioxide · Pt nanoparticles · Carbon supports · Methanol electrooxidation · X-ray diffractometry

E. E. Said-Galiyev · A. Y. Nikolaev · A. R. Khokhlov
A.N. Nesmeyanov Institute of Organoelement Compounds,
Russian Academy of Sciences,
Vavilov Str. 28,
Moscow 119991, Russia

E. E. Levin (✉) · E. K. Lavrentyeva · M. O. Gallyamov · S. N. Polyakov · G. A. Tsirlina · O. A. Petrii · A. R. Khokhlov
Lomonosov Moscow State University,
Leninskie Gory, 1-Str.3,
Moscow 119992, Russia
e-mail: levin@elch.chem.msu.ru

S. N. Polyakov
Technological Institute for Superhard and Novel Carbon Materials,
Tsentral'naya Str. 7a, Troitsk,
Moscow Region 142190, Russia

Introduction

Application of supercritical fluids to metal dispersion is an attractive technique: it is believed to support the formation of rather small particles with narrow size distribution and homogeneous distribution along support due to the specific mechanisms of precursor adsorption. In addition, nanostructural metal properties are expected to be independent of its loading. However experimental confirmations still look occasional and insufficient. Catalysis and electrocatalysis seem to be a natural field for resulting materials with relatively low coalescence degree [1–7]. However supercritical technologies (SCT) are usually expensive (as compared with conventional approach, i.e. liquid-media impregnation with subsequent chemical reduction or thermal decomposition). This is why SCT approach can be considered as something reasonable only if the functional properties of catalysts are advantageous. Doubts concerning this point arise in particular from the nature of Pt-containing reagents used in SCT: for the most typical precursors, organic fragments formed from ligands tend to adsorb strongly and irreversibly on Pt.

Recently the electrochemically active surface area and electrocatalytic activity of SCT-Pt were briefly reported [1, 2, 4, 6], as well as the results of fuel cell tests [5]. However these data remain too fragmentary for quantitative comparison of usual and SCT-produced catalysts. Completely

missed point is a steady-state specific activity, the property one can never estimate from cyclic voltammetry (like in Ref. [4]). In contrast to hydrogen or oxygen reactions, for organic fuels oxidation the activity cannot be judged from exchange current density (like in Ref. [1]). The most crucial problem of steady-state methanol electrooxidation is self-poisoning. In what follows, we pay special attention to this problem and accent another very important point, the reliable material characterization necessary to correlate nanostructural and functional properties. TEM data can be misleading in the absence of an appropriate statistical treatment. To avoid speculations when treating XRD data, one needs to take into account the overlap of carbon and platinum reflections and to apply the 'beyond-Scherrer" models when analysing the reflection profiles for so small particles. Combination of thoroughly treated TEM and XRD allows to get more solid knowledge of nanostructure.

We report below a set of comparative data for commercial HiSpec (Johnson Matthey) and original SCT-produced platinum catalysts on carbon blacks. Despite of the pronounced initial poisoning with organic co-products (or probably just due to decrease of self-poisoning with methanol in the presence of these foreign adsorbates) some of catalysts under study demonstrate the remarkable specific activity under steady-state conditions.

Experimental

Catalysts preparation and characterization

The precursor for SCT dimethyl(1,5-cyclooctadiene)platinum(II) $Pt(CH_3)_2COD$ (Pt content ~58%), Aldrich) was used without further purification. This reagent with decomposition temperature of 140–200 °C [8] was chosen because of its rather high solubility in supercritical CO_2 ($scCO_2$): 15 mg cm^{-3} at 80 °C, 27.6 MPa [2].

Two carbon supports were tested, acetylene black AC-1 (OOO VNIIGAZ, Russia) and Vulcan XC72R (Cabot Corp., USA). The AC-1 material is more hydrophobic and can be dispersed in water only after surface oxidative treatment, or surfactants admixing (Kotosonov AS, private communication). The specific surface area of 120–150 $m^2 g^{-1}$ was determined for this material by BET technique (Quantochrome NOVA 220e, Quantochrome Instruments) (Valetsky PM, private communication). Vulcan XC72R is more oxidized (contains polar groups at the surface) and has larger BET surface area (210–250 $m^2 g^{-1}$ [9, 10]).

High purity carbon dioxide (99.997 vol.%, GOST 8050-85) was used as a solvent. High-pressure (up to 35 MPa) setup for operations with supercritical carbon dioxide was constructed in the Institute of Mineralogy, RAS, with the use of armature from High Pressure Equipment, USA. The experimental setup consisted of a pressure generator connected to a high-pressure system containing the lines of capillary tubes, manometers, set of valves and a reactor (diameter of 2 cm, and an internal volume of 23 cm^3), see [11] for details.

Fabrication procedure looked as follows. The reactor was loaded with 0.1–0.25 g of carbon black and 0.1–0.3 g of $Pt(CH_3)_2COD$. After sealing, CO_2 was first blown through the reactor for 5 min, and then the temperature was increased up to 120 °C. Then 25 MPa pressure was applied. In some experiments, the reagents were mixed with a steel Teflon-coated stirring rod. The reactor was placed into thermostatically controlled bath (±0.5°) positioned on RCT basic magnetic mixer "RCT basic" IKA-Werke GmbH (silicone oil No 5). The exposure was performed during 6 h in order to ensure both the equilibration of the organic precursor solution in $scCO_2$ and the uniform distribution of solution components at the surface of carbon support. After 6-h long exposure the reactor was cooled down to the room temperature, and the pressure was decreased by opening the reactor valve.

The resulting product was carbon powder with immobilized precursor. For platinum reduction, this powder was heat treated in the same reactor under either Ar or CO_2 flow (20–30 cm^3 min^{-1}). Reduction took 3–6 h at 150–230 °C under 0.3–30 MPa. Summary of synthesized catalysts is presented in Table 1. It should be noted that combination of high pressure and Ar atmosphere resulted (at least from the first attempt) in formation of coarse-dispersed platinum. The reasons are not completely clear at this stage. In what follows we discuss only the samples with crystal size not exceeding 20 nm.

Samples characterization included elemental analysis (Pt; for some samples C and H as well), TEM, and XRD.

Elemental analysis was performed using X-ray fluorescence spectrometry, Zeiss Jena VRA-30, with the accuracy ±0.3%. C and H were determined after burning in air at 850–900 °C or in oxygen at 1,800 °C.

For TEM analysis, the dry powder was applied onto a copper grid covered with a polyvinyl (commercial Formavar, Plano GmbH) supporting film. An excess of the powder was removed by blowing with air. We avoided any wet treatment, to exclude possible disturbance of Pt particles on the carbon support due to capillary forces in the course of sample preparation. The micrographs were taken using a LEO 912 AB microscope (LEO/Carl Zeiss, Germany) as digital images with informational density of 2,048×2,048 points. Image analysis was performed using FemtoScan image processing software (ATC, Russia): the diameter of the individual visualized Pt particles was measured, 250 different particles were analyzed for each sample (N=250). The data array of the measured diameter (d_i) values was further numerically analyzed using Origin-

Table 1 Summary of synthesis conditions for various catalysts: temperature (*T*), pressure (*P*), time (*t*)

Sample	Support	Incorporation conditions in $scCO_2$				Reduction conditions			wt.% Pt, assumed/found
		T, ºC	*P*, MPa	*t*, h	Medium	*T*, ºC	*P*, MPa	*t*, h	
A	XC72R	120	25	6	Ar	230	0.3–0.4	8	19/20
B	AC-1	120	25	6	Ar	180	0.3–0.4	8	30/26
C	AC-1	120	25	6	Ar	180	0.3–0.4	8	30/27
D	AC-1	120	25	6	Ar	150	0.3–0.4	8	31/28
E	AC-1	120	25	6	CO_2	150	30	8	30/29
F	AC-1	120	25	6	CO_2	150	6	8	31/30
G	AC-1	120	25	6	Ar	150+200	0.3–0.4	6+2	39/38

Pro 7.5 software in order to calculate a mean value of the diameter and its standard deviation, as well as to draw histogram of diameter distribution. Besides, we estimated the specific surface of Pt (*S*) using the following equation:

$$S = \frac{6\sum_{i=1}^{N} d_i^2}{\rho \sum_{i=1}^{N} d_i^3}$$

where ρ is platinum density (21.45 gcm^{-3}).

Powder diffraction data were collected in step scan mode using RIGAKU D/max RC powder diffractometer equipped with a scintillation detector (Bragg–Brentano geometry (θ–2θ scan), flat graphite crystal analyser). Samples were inked onto the self-made zero-background sample holder. It is essential to use this type of holders for low-absorbing samples, when the transparency effects are significant [12]. XRD patterns of the carbon blacks were recorded in the range 2θ=10–125° using a step Δ2θ=0.05° and CuK_α radiation. XRD patterns of the catalysts were recorded in the range 2θ=10–80° using a step Δ2θ=0.05° and MoK_α radiation. At least 10^5 counts above background level for the strongest reflections were collected for each catalyst. For phase identification, database [13] was used. The instrumental broadening was determined using standard reference material LaB_6 (NIST SRM660a). Zero shift was refined for LaB_6 pasted in the same manner as the samples under investigation and later was used as a constant in the course of catalysts structure refinement.

Cell parameters were refined by the Rietveld method [14] using the MAUD program [15]. Crystallite sizes and root-mean-square strain were estimated using two-stage approach [16] integrated into MAUD. Spherical shape of the coherently diffracting domains was assumed. In order to compensate carbon black contribution to XRD patterns of catalysts, individual carbon black XRD patterns were fitted with the sets of pseudo-Voigt peaks, which were later considered as a background in the course of refinement of catalysts structure.

Electrode preparation and electrochemical measurements

Catalyst powder was dispersed ultrasonically in ethanol (2.5 mgL^{-1}) to obtain a homogeneous black suspension. Aliquots, 20 μL of this suspension were pipetted onto a square-shaped (10-mm side) pyrolitic graphite supports. After 20 min drying in air these electrodes were covered with 10 μL of 0.5 wt.% Nafion (Aldrich) to fix the sample, and dried again in air for 20 min. To avoid possible underestimation of specific surface area of Pt induced by partial screening of Pt particles in inhomogeneous mixture, three portions of suspension for each catalyst were prepared, and the data for corresponding electrodes were compared. The highest specific surface area found for each catalyst is presented below.

Electrochemical measurements were carried out with an EG&G potentiostat PARC 273 and Autolab PGSTAT30 in three-electrode cell at 25 °C. The counter electrode was Pt foil, and the reference electrode was saturated calomel electrode connected to the cell via a Luggin capillary. Potentials *E* hereinafter are given versus RHE. True surface areas of Pt (*S*) in the samples were determined coulometrically from hydrogen desorption and from carbon monooxide desorption regions of cyclic voltammograms (CV). In the former case (*S*(H)) CVs were registered in 0.5 M H_2SO_4 solution (after deaeration with Ar for 90 min) at 0.10 $V{\cdot}s^{-1}$ in 0.06–1.24 V potential interval. Potential was cycled until a stationary voltammogram was obtained (usually in the fiftieth cycle). Very slow evolution of CVs was observed in the course of stabilization. Minor "excessive" current in the double layer region decreased systematically in subsequent cycles, and simultaneous increase of H-UPD charge and improvement of CVs shape in the hydrogen region took place. This evolution is not specific for any type of organic impurities. For independent determination of the true surface area (*S*(CO)), CO was adsorbed from CO-saturated solution (10 min), and then the electrolyte was purged with Ar (90 min) to remove dissolved CO. CVs were registered at 0.02 Vs^{-1} in 0.06–1.44 V potential

interval. The specific charge of 420 μC·cm^{-2} was assumed, corresponding to desorption of the monolayer of linear CO adsorbate. If bridged CO species existed in adlayer, the *S* (CO) value could be under-, but not overestimated. We suppose that possible relative error introduced by assuming linear form of CO is close for various catalysts, and should not affect the comparative characterization in the series.

To check a possible surface contamination with the products of ligand destruction, test voltammetric experiment in 0.5 M H_2SO_4 on Pt foil (0.25 cm^2) covered with 10 μL of COD was done.

Steady-state polarization curves were measured in 0.1 M CH_3OH+0.5 M H_2SO_4 solution under potentiostatic mode (the current was considered as already stationary if its further change was less than 0.7% in 60 s). At each potential the current transients were collected. The open circuit potential was used as a starting value, then the potential step to 0.54 V was applied, with subsequent 30–40 mV steps toward more positive potentials. The shape of observed transients is not discussed in details here; the trends of current vs. time behavior are determined by interfacial charging of Pt and carbon support, as well as by the changes in surface coverage with strongly bound organic adsorbate that slows down the process.

MilliQ water, H_2SO_4 (Merc, GR for analysis), Nafion Perfluorinated Ion-Exchange Resin, 5 wt.% Soln. in Lwr. Aliph. Alcohols/H_2O (Aldrich), HCl (Merc, GR for analysis) and CH_3OH (distilled) were used.

Results and discussion

Structural characterization

XRD patterns of two different carbon blacks are shown in Fig. 1. One can see that the patterns of both supports are very similar and can be assigned to graphite-2H/graphite-3R mixture (ICDD PDF2 cards #26-1079 and #41-1487 [13]). The peaks are broader for Vulcan XC72R carbon black, indicating either smaller crystallite size, or (and) the higher concentration of stacking faults.

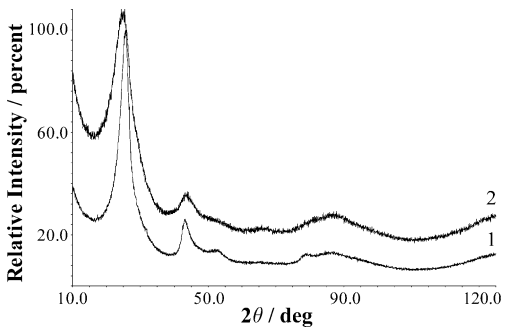

Fig. 1 XRD patterns of AC-1 (*1*) and Vulcan XC72R (*2*). CuK_α radiation

TEM images and corresponding size distributions of SCT-produced (A, G) and commercial catalysts (HiSpec 3000, HiSpec 4000) are presented in Figs. 2 and 3. We have chosen samples A and G for comparison with reference commercial samples to consider close Pt loadings (low and high, respectively). Rather similar size distributions were observed for low loading (HiSpec 3000 and sample A, ~20 wt.% Pt, Fig. 3a, b), when for higher loadings (HiSpes 4000 and sample G, ~40 wt.% Pt) the pronounced difference was found. Maximum of distribution obtained for original sample G corresponds to smaller particle size, and distribution is more narrow (Fig. 3d) as compared with HiSpec 4000 (Fig. 3c). It should be also mentioned that Pt loading in commercial catalysts affects strongly the homogeneity of the samples and the mean particle sizes (*D(TEM)*): the increase of Pt loading results in formation of larger particles (more than 5 nm in diameter) and in a shift of the mean particle size from 2.1 to 2.8 nm (Fig. 3a, c; Table 2). The effect of loading on *D(TEM)* of SCT-produced catalysts is less significant (from 2.0 to 2.2 nm) (Fig. 3b, d; Table 2). TEM data for all synthesized catalysts (Table 2) correspond to mean particle size from 2.0 to 2.4 nm. This probably means that our fabrication protocol allows to produce rather small particles with narrow size distribution independently of Pt loading, at least in 20−40 wt.% range. This is not the case typical for any SCT-produced catalysts reported in the literature: for supported platinum nanoparticles on various solids, including silica and γ-alumina [3] and carbon aerogels [8], higher metal content results in a larger size of particles. For 30 wt.% Pt on carbon, the total interval of particle size (1–5 nm) is similar to our findings, and distribution maximum corresponds to 2.8±0.7 nm (it agrees with the highest value we found for our samples) [8]; slightly wider interval was found in Ref. [6]. Comparison with SCT-produced Pt catalysts on carbon nanotube supports [1, 17, 18] demonstrates more pronounced difference: for 25 wt.% Pt, the reported distribution was shifted to 5–10-nm interval [1].

We can assume that particle formation and growth is primarily governed by the interaction of organometalic precursors with the support, and that carbon black supports allow the formation of particles at higher number of surface centers, being a perspective support for SCT-produced 2–2.5-nm Pt particles with narrow size distribution. However the latter feature remains less reliable because our statistics is limited to 250 particles. The analysis of TEM data involving up to 900 particles [5] resulted in essentially different shape of distribution (less symmetric, with very high contribution of smaller particles). We should point out that the authors of Ref. [5] used supercritical methanol instead of $scCO_2$ as a fluid.

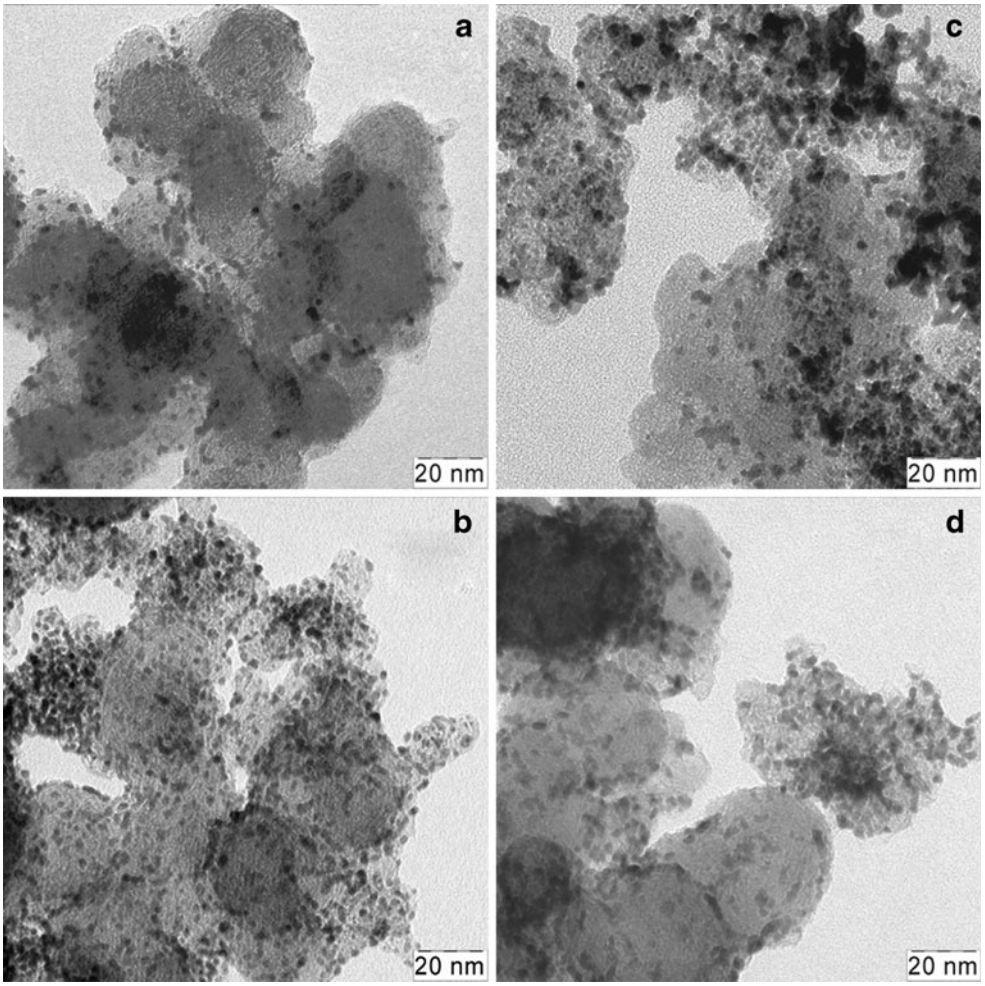

Fig. 2 TEM images for synthesized (A (**b**), G (**d**)) and commercial (HiSpec 3000 (**a**), HiSpec 4000 (**c**)) catalysts. Pt content is ca. 20% (**a**, **b**) and ca. 40% (**c**, **d**)

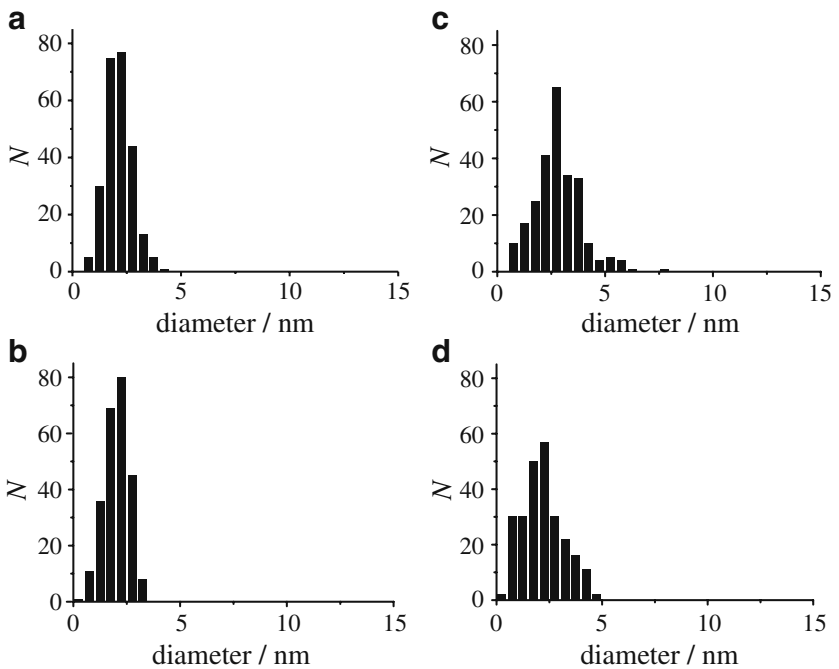

Fig. 3 Size distributions obtained from TEM data for synthesized (A (**b**), G (**d**)) and commercial (HiSpec 3000 (**a**), HiSpec 4000 (**c**)) catalysts. Pt content is ca. 20% (**a**, **b**) and ca. 40% (**c**, **d**). *N* is the number of particles of certain size (the total number is ca. 250)

Table 2 Mean sizes of Pt particles (D(TEM)) obtained from size distributions from TEM data, sizes obtained from Gauss approximation of mass/size distributions (D(TEM, wt.)); cell parameters (a(Pt)), reflection widths (FWHM), root-mean-square strains (r.m.s. strain), average crystallite sizes for XRD patterns (D(XRD)); specific surface areas (S(TEM)) of Pt particles obtained from size distributions from TEM data, specific surface areas determined coulometrically from the CO desorption region (S(CO)) of CVs, specific surface areas (S(XRD)) of Pt particles obtained from XRD data are given

Sample	D(TEM), nm	D(TEM, wt.) nm	a(Pt), Å	r.m.s. strain	D(XRD), nm	S(TEM), $m^2 g^{-1}$	S(CO), $m^2 g^{-1}$	S(XRD), $m^2 g^{-1}$
A	2.0±0.6	2.5±0.1	3.923±0.001	0.0185±0.0001	2.4±0.1	120	90	116±5
B	2.0±0.5	2.3±0.1	3.9217±0.0004	0.0143±0.0001	8.1±0.1	130	80	34±1
C	2.0±0.8	3.0±0.1	3.9309±0.0008	0.0178±0.0002	3.2±0.1	100	80	87±3
D	2.3±0.9	3.2±0.1	3.9184±0.0003	0.0115±0.001	9.5±0.1	90	40	29±1
E	2.4±1.0	2.9±0.2	3.9206±0.0003	0.0082±0.0001	5.1±0.1	80	60	54±2
F	2.0±0.7	2.5±0.1	3.9246±0.0005	0.0159±0.0002	4.3±0.1	120	70	65±3
G	2.2±1.0	3.4±0.1	3.9203±0.0003	0.0104±0.0001	3.8±0.1	90	60	73±4
HiSpec 3000	2.1±0.6	2.6±0.1	3.927±0.001	0.0230±0.0006	4.6±0.1	110	90	60±2
HiSpec 4000	2.8±1.1	3.6±0.1	3.9211±0.0002	0.0111±0.0004	7.4±0.1	80	50	37±1

XRD patterns for some SCT-produced catalysts and commercial samples are presented in Fig. 4. The difference in reflection widths for synthesized and commercial samples is well pronounced. Corresponding average sizes of the coherently diffracting domains (D(XRD)) are given in Table 2. To compare XRD and TEM data we recalculated size distributions to deal with mass fractions. Recalculated distributions are necessary for comparison with D(XRD) since Scherrer equation provides volume-weighted values [16]. The resulting broad distributions were fitted by Gauss functions; the size values corresponding to thus obtained maximums D(TEM, wt.) are also listed in Table 2. In contrast to HiSpec catalysts, SCT-produced catalysts demonstrate no direct correlation of Pt loadings and D(XRD). In addition, average crystallite sizes for A and G samples are smaller than for corresponding commercial reference samples with close loadings, namely HiSpec 3000 and HiSpec 4000. The following reasons of advantageous SC technology can be assumed. Firstly, scCO2 is an excellent wetting agent in respect to carbon black surface, with its wetting ability independent on the surface hydrophilicity, so no problems arise with initial homogeneous distribution of the precursor along the surface, and the thickness of precursor layer is fixed by the quantity of Pt-containing reactant. Secondly, the capillary forces are absent when CO_2 is removed in the course of reactor decompression, so the immobilized precursor is not removed from the surface.

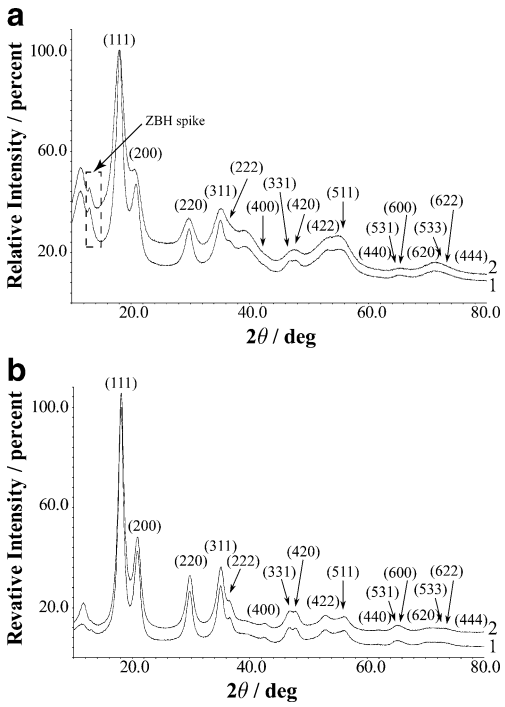

Fig. 4 XRD patterns for samples with low (**a**) and high (**b**) Pt loadings: HiSpec 3000 (**a**, curve 1), HiSpec 4000 (**b**, curve 1), A (**a**, curve 2), G (**b**, curve 2). MoK_α radiation

Basically, the cell parameters and zero shift are highly correlated [19]. For nanocrystalline systems this correlation is so pronounced that even when dealing with calculated patterns one cannot obtain back model parameters using standard Rietveld refinement routine [20]. In this study we determined zero shift by measuring the positions of LaB_6 peaks pasted onto zero-background holder, and used this value later as a reference. It can be seen that all cell parameters are in fact very close to the values for bulk platinum (a=3.9231 Å [13]), i.e., no pronounced lattice compression is observed, in contrast to electrochemically grown nanocrystals [21]. Any attempt of simultaneous refinement of zero shift and cell parameters resulted in drastically lower cell parameters and unrealistically high zero shift values. In this case the error of cell parameter determination is at least one order of magnitude higher than least-squares error given in Table 2. The reason is that all

peaks are very broad, and the precision of peak position determination is rather low.

It can be observed that all mean-numerical (D(TEM)) values are lower than D(XRD), which is a common feature for systems with wide particle size distributions [22]. It is easy to observe that D(TEM, wt.) values for all samples under study are lower than (or equal to) D(XRD). This fact indicates the absence of crystallite coalescence at least for significant fraction of visualized particles, in contrast to earlier observations for carbon-supported nanoparticles of platinum [4, 8]. Crystals coalescence usually results in the formation of defective regions (intergrain boundaries) and can also induce the pronounced defectiveness of nm-size grains. Both features are well pronounced for electrodeposited platinum [21], and correlate with Pt electrocatalytic activity towards methanol oxidation [23].

XRD demonstrates that the reproducibility of synthetic procedure is still not very high (e.g., if one compares the samples B and C). However the difference between our data and the alternative catalysts is evident, and at this stage we concentrate on the basic structural features responsible for the functional properties of catalysts, in order to work out more perfect synthetic strategy. The results for all samples excluding A and C demonstrate the pronounced deviation from TEM data, most probably because of statistical reasons mentioned above. Less successful sample D, with higher D(XRD), demonstrates that the decrease of reduction temperature can be crucial. This finding does not cancel our conclusions, but demonstrates the necessity to fix the ranges of fabrication parameters for future improvement of SCT technology.

In addition to size distribution, lattice strain is an important structural parameter. Strain values found for SCT series are intermediate as compared with strain of Pt in two commercial samples. The highest strain in the series is found for samples A and C. At this stage we simply fix this finding. Our next steps are (1) to estimate the degree of coalescence from microscopic data and electrochemically available true surface area, (2) to test electrocatalytic activity, and (3) to consider its correlations (if any) with nanostructural features reported above.

XRD characterization of similar SCT materials is recently reported [6], with simplified treatment of reflections broadening (both instrumental broadening and strains are ignored). We assume that the misleading results can also appear when size is estimated from one reflection, in contrast to our study (due to the use of Mo radiation we were able to register 19 reflections). This can be a reason why slightly larger crystallite size (3.7 nm) was found in [6] as compared with our results. At the same time, the apparent true surface areas of supported platinum fabricated by the authors of Ref. [6] are several times lower, as we can roughly estimate form comparison of CV data (Fig. 4 in Ref. [6]) and the reported loadings. Probably the higher temperature of precursor decomposition applied in Ref. [6] resulted in increased surface diffusion rate and accelerated coalescence of platinum particles. The problem of the surface area determination for SCT-fabricated Pt is specially addressed in the next section.

Specific surface area of Pt in catalysts

Voltammograms of sample A (~20 wt.% Pt) and commercial catalysts HiSpec 3000 (~20 wt.% Pt) are compared in Fig. 5a. Curves 2 and 3 for sample A were registered before CO adsorption and after CO desorption respectively. CO adsorption–desorption resulted in significant purification of Pt surface initially contaminated with organic species (most probably these species were the products of ligand destruction in the course of catalyst fabrication). For catalysts SCT-produced from organic precursors, voltammograms in the hydrogen adsorption region are always featureless [1, 4], like curve 2 in Fig. 5a. At the same time, when inorganic (chloride) precursor is used in SC technology, the shape of voltammogram in the hydrogen region is very close to the shape known for pure Pt [21]. Among poisoning by-products, cyclooctadiene (COD) can be expected first of all [24]. To check this assumption we

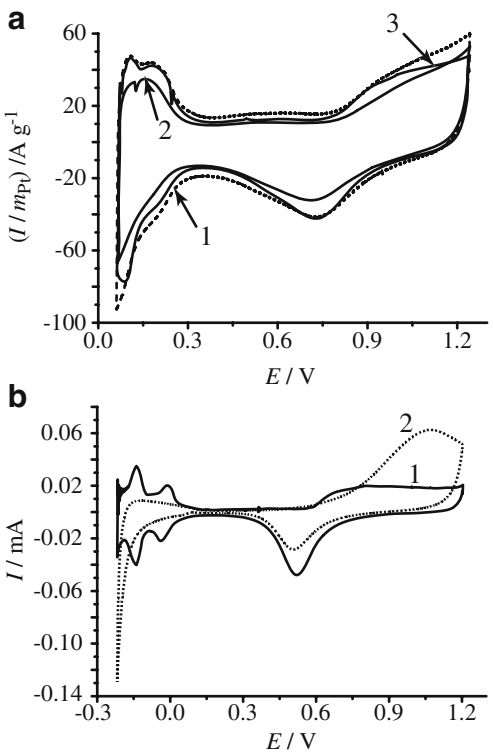

Fig. 5 Cyclic voltammograms for samples: HiSpec 3000 (**a**, *curve 1*), A (before (**a**, *curve 2*) and after (**a**, *curve 3*) CO adsorption–desorption procedure), and Pt foil (before (**b**, *curve 1*) and after (**b**, *curve 2*) modification with COD)

covered Pt foil with COD (Fig. 5b, curve 2) and compared the CVs for pure (Fig. 5b, curve 1) and thus modified Pt foil. This test experiment confirmed the significant poisoning of Pt with COD. In subsequent experiments we were able to purify the surface of COD-modified foil by means of CO desorption. This means that CO species adsorb stronger (at least at low potentials) as compared with contaminating by-products, and the latter are forced out. Later CO undergoes oxidative desorption, and the surface appears to be pure. Independently on details of this competitive adsorption we believe that poisoning in the course of SCT is not a crucial problem.

Specific surface areas (S(H), S(CO)) of Pt determined from voltammetry are collected in Fig. 6. Basically S(H) values for our catalysts are higher or comparable with S (CO) for commercial samples. However these values are typically lower than the expected highest possible specific surface areas estimated from TEM (S(TEM)) or XRD (S (XRD)). S(TEM) and S(XRD) values can be considered as the reasonable estimates of the area of non-coalesced particles only if size distribution of particles is very narrow (Table 2). Experimental value should be lower because of partial screening of Pt surface resulting from either coalescence of crystals or from too narrow pores between them [21], complicating electrolyte penetration. On the other hand, S(H) values for the majority of SCT-catalysts are lower or comparable with the same values for commercial samples, probably because of stronger contamination and inability of hydrogen adatoms to compete with strongly adsorbed organic species. Note that B, D, F samples were not purified by CO adsorption–desorption procedure, and corresponding S(H) values are most probably underestimated.

Using TEM and XRD data we can roughly estimate the portion of screened surface from the ratio of experimental S (CO) values and expected values for ensembles of spheres.

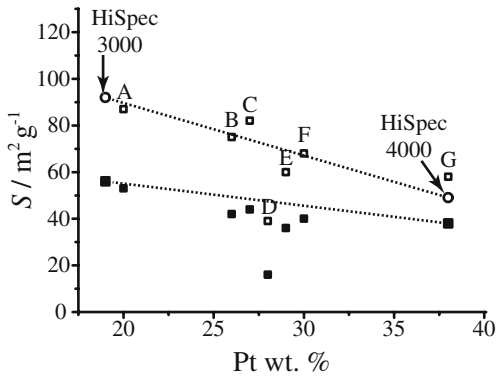

Fig. 6 Specific surface areas of Pt for SCT-produced and commercial samples, as determined coulometrically from the H (*filled squares*) and CO (*open squares*) desorption regions of CVs. The data for HiSpec (*open circles*) are reported by supplier (Johnson Mattey)

Of course this is possible only if the calculated values S (TEM) and S(XRD) exceed S(CO), which is not the case for S(XRD) obtained for majority of samples. This is not surprising because XRD misses the data for the smallest particles, in contrast to TEM, missing some rare large particles. On the basis of results going from both techniques we can conclude that the portion of screened surface never exceeds 0.3–0.4. These values are typical for the most loose Pt electrodeposits, when more typical values for the latter are up to 0.7 [21], i.e. our SCT-Pt samples are not strongly coalesced. The coalescence degree for SCT-Pt demonstrates more weak dependence on Pt loading as compared with HiSpec (Table 2).

Electrocatalytic methanol oxidation

Current transients for methanol oxidation normalized per Pt weight (*m*) (Fig. 7, left column) correspond to potentials of 0.54 (a), 0.59 (b), 0.64 (c), and 0.69 (d) V, i.e., to a typical region of Pt self-poisoning. Comparison of these transients for samples A, C, G, E with the transients of commercial samples demonstrate that both initial and steady-state currents for SCT-catalysts are higher, and the difference is sometimes significant. For low-loaded samples (A, HiSpec 3000), current maxima always exists (excluding one curve for HiSpec 3000 in Fig. 7a). For high Pt loading (G, HiSpec 4000), the difference is more pronounced: HiSpec 4000 always demonstrates monotonous current decrease, when for SCT-catalyst this behavior takes place only at the lowest potential. The decrease of current after maxima for all SCT-catalysts is the same or slower than for commercial catalysts, never sharper. The most specific is sample C, with its current plateau instead of current decrease. In general we can conclude less pronounced self-poisoning of SCT-catalysts, especially at low potentials (being most interesting for applications). To demonstrate weaker self-poisoning more clearly, we present all the transients normalized per initial current I_0 (Fig. 7, right column). To clarify the reasons of less pronounced self-poisoning of SCT-catalysts, additional mechanistic study is required. In some experiments the CVs in background solution were run after electrocatalytic tests. These CVs typically demonstrate the decrease of hydrogen adsorption/desorption charge, but the effect is not characteristic, i.e., one can hardly separate the effects of methanol destruction products and any foreign adsorbate (e.g., the residual surface contaminations originating from the precursor). One cannot exclude that this sort of contaminations plays poison-protecting role.

Steady-state polarization curves of methanol oxidation (Fig. 8) are plotted for current densities normalized per true surface area (Fig. 8a, c) and per Pt weight (Fig. 8b). The specific activity is higher for all SCT-catalysts as compared with both HiSpec samples, and this conclusion is indepen-

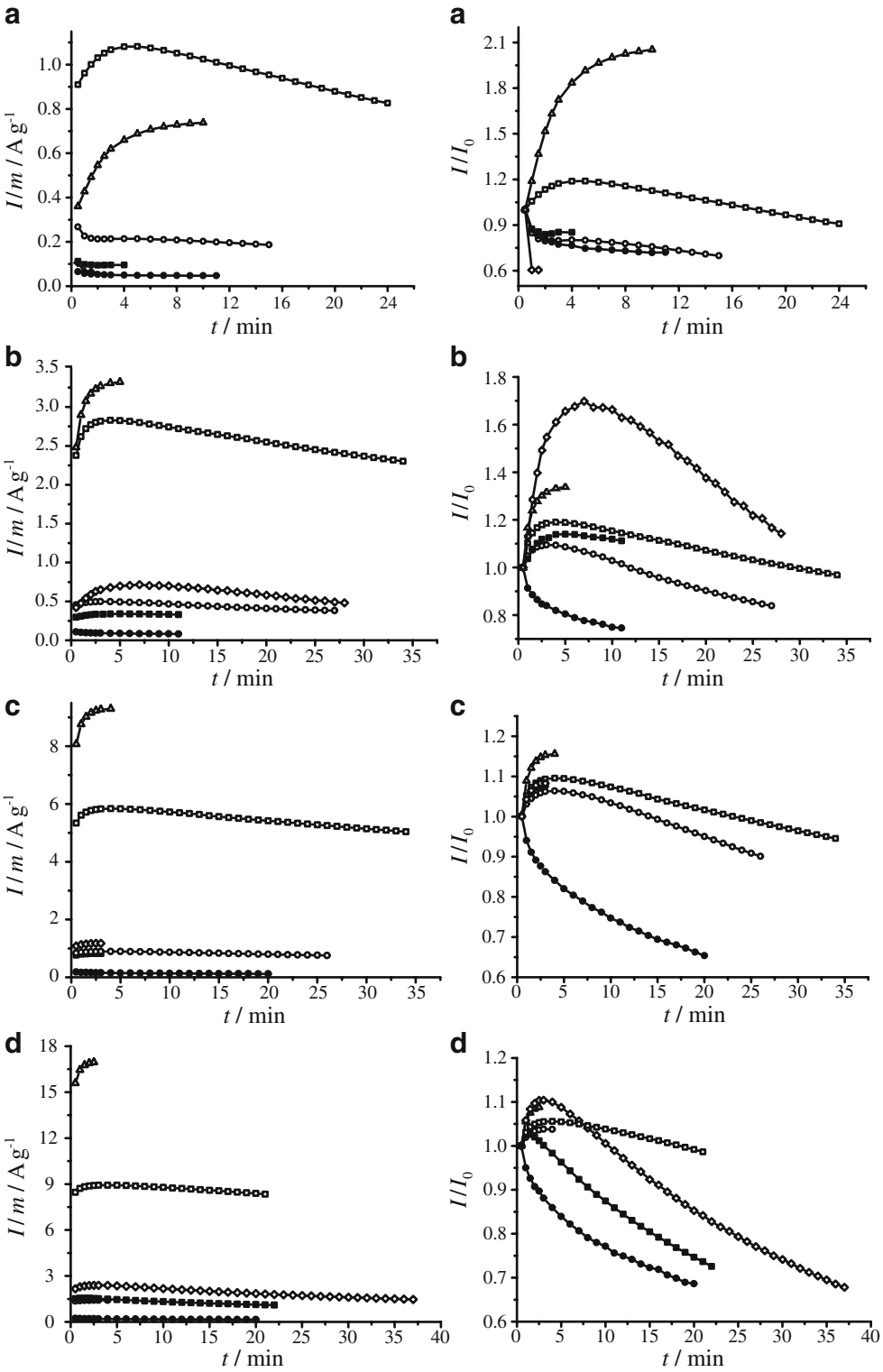

Fig. 7 Current transients for methanol oxidation for SCT-produced (*open symbols*: *squares* (A), *circles* (G), *triangles* (C), rhombs (E)) and commercial (*filled symbols*: *squares* (HiSpec 3000), *circles* (HiSpec 4000)) samples. Transients are registered at different potentials (0.54 V (**a**), 0.59 V (**b**), 0.64 V (**c**), 0.69 V (**d**)) and normalized per Pt weight (*left column*) and per initial current value (*right column*)

dent on the type of normalization (per true surface area or per weight). The difference in activity approaches one order of magnitude. For high loading, the difference is more pronounced at higher anodic potentials (Fig. 8c). The highest specific activities are found for the most defective and most dispersed samples A and C (in combination both factors result in the most wide reflections in the series, a feature easily observed without any model treatment). As the degrees of crystal coalescence for samples A and C are rather low, the defectiveness hardly results from grain

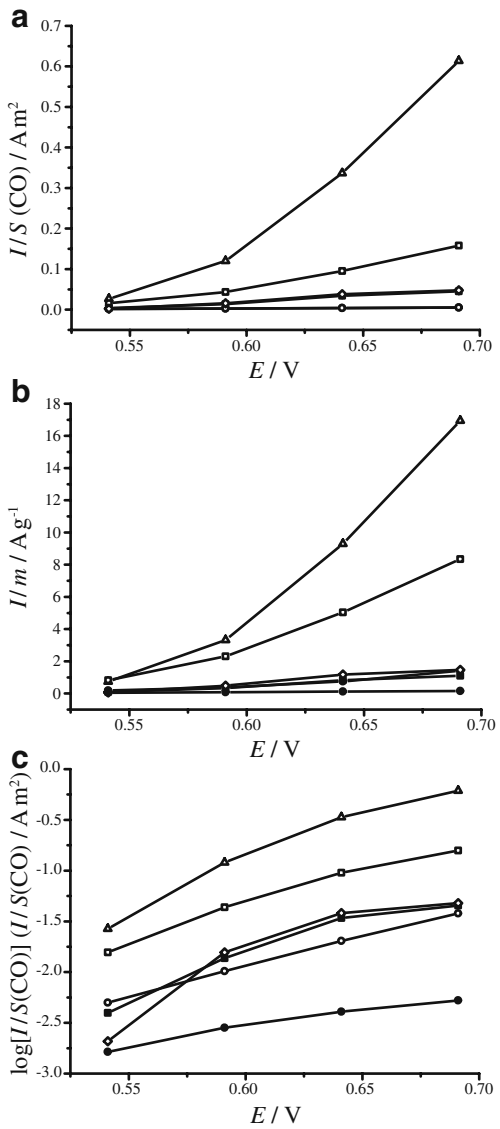

Fig. 8 Fragments of steady-state polarization curves of methanol oxidation normalized per true surface area (**a**, **c**) and per weight (**b**) for SCT-produced (*open symbols*: *squares* (A), *circles* (G), *triangles* (C), *rhombs* (E)) and commercial (*filled symbols*: *squares* (HiSpec 3000), *circles* (HiSpec 4000)) catalysts

boundaries formation and should be assigned to Pt crystals themselves.

Conclusions

Our data on SCT-platinum demonstrate some advantages of these materials as compared with catalysts prepared by other means. At the same time the detailed structural characterization discovers some difference for ca. 20, 30, and 40 wt.% Pt loadings. It confirms that one should not simultaneously look for any straightforward correlation with a single macroscopic parameter: most important are correlations with lattice and nanostructural features.

Some poisoning of SCT-electrocatalysts with the species remaining from the ligand destruction was detected. However this poisoning is apparently not an issue, at least for applications related to methanol reaction. Anyway, for other applications other Pt-containing ligands may be applied. We selected $Pt(CH_3)_2COD$ only due to its commercial availability and high solubility in $scCO_2$. Some fluorinated ligands would be more preferable, which can be specially synthesized for the particular applications. Another possible approach remains using of water-soluble Pt precursors for an impregnation stage [25], with adding the fluorinated surfactants to stabilize water-in-$scCO_2$ dispersion.

Application of SCT gives the specific possibilities to vary lattice defects concentration and particle size. As the nature of Pt formation processes is completely different than for electrodeposition [21, 23], one can judge about the role of lattice imperfections in electrocatalysis in more general sense. We cannot treat our XRD data exactly in the manner used in [21] because of lower loading and specific support contribution. In frames of two-stage approach [16] used in this work we can only extract some weighted strain value. Conventional approach is to relate this strain parameter to concentration of dislocations [26] or any other 'strain' effect [26], but in real materials more than one type of defects can coexist. For more detailed characterization, one should apply HRTEM technique able to resolve local particle structure, and combine it with the state-of-the-art powder diffraction modeling, such as Whole Powder Pattern Modeling [27].

We conclude that for two groups of catalysts with different typical size of particles (typically 2–3 nm for SCT and 15–20 nm for electrodeposited Pt) defectiveness correlates with catalytic activity towards methanol oxidation in qualitatively similar manner.

Further penetration into the problem requires application of high resolution microscopic techniques to study the geometry and mutual location of defects. The most challenging aspect of this problem is to separate defects located at grain boundaries of coalesced crystals and lattice defects in crystals themselves. SCT-catalysts with their rather low degree of coalescence provide useful contribution to future understanding. It is rather probable that just defective crystals, not boundaries, are responsible for catalytic activity. For more coalesced crystals, like those studied in [21, 23], boundaries can be responsible for additional lattice compression and defectiveness induced by this factor.

From synthetic point of view, low-pressure Ar SCT-technique looks most promising. Specific optimization of temperature is most probably required for any certain type of carbon black support.

Acknowledgements The work was done under financial support from the National Innovation Company New Energy Project and also was partly supported by RFBR, project 08-03-00854-a. The authors are grateful to Prof. P.M. Valetsky and A.S. Kotosonov for the samples of acetylene black AC-1 and fruitful discussions. M.O.G. and E.E.S.-G. are grateful to Russian Academy of Sciences for the support within Presidium's Basic Researches Program No 27.

References

1. Lin Y, Cui X, Yen C, Wai C (2005) J Phys Chem B 109:14410–14415
2. Zhang Y, Erkey C (2005) Ind Eng Chem Res 44:5312–5317
3. Zhang Y, Kang D, Saquing C, Aindow M, Erkey C (2005) Ind Eng Chem Res 44:4161–4164
4. Bayrakceken A, Smirnova A, Kitkamthorn U, Aindow M, Turker L, Eroglu I, Erkey C (2008) J Power Sources 179:532–540
5. Taylor AD, Sekol RC, Kizuka JM, D'Cunha S, Comisar CM (2008) J Catal 259:5–16
6. Ang S-Y, Walsh DA (2010) J Power Sources 195:2557–2563
7. Erkey C (2009) J Supercrit Fluids 47:517–522
8. Saquing C, Cheng T-T, Aindow M, Erkey C (2004) J Phys Chem B 108:7716–7722
9. Kaiser J, Simonov PA, Zaikovskii VI, Hartnig C, Jorissen L, Savinova ER (2007) J Appl Electrochem 37:1429–1437
10. Klinedinst KA (1985) J Electrochem Soc 132:2044–2050
11. Said-Galiev EE, Vygodskii YaS, Nikitin LN, Vinokur RA, Khokhlov AR, Pototskaya IA, Kireev VV, Schaumburg K (2004) Polym Science A 46:377–380
12. Misture ST, Chatfield LR, Snyder RL (1994) Powder Diffr 9:172–179
13. PCPDFWin (ver. 1.30, JCPDS ICDD, Swarthmore, PA, USA, 1997
14. Young RA (Ed.) (1993) The Rietveld Method. IUCr Monograph No.5, Oxford University Press, New York.
15. Lutterotti L, Matthies S, Wenk H-R (1999) IUCr: Newsletter of the CPD 21:14–15
16. Delhez R, Keijser TH, Langford JI, Louer D, Mittemeijer EJ, Sonneveld EJ (1993) Crystal imperfection broadening and peak shape in the Rietveld method. In: Young RA (ed) The Rietveld method. Oxford University Press, New York, pp 132–166
17. Bayrakceken A, Kitkamthorn U, Aindow M, Erkey C (2007) Scr Mater 56:101–103
18. Yen CH, Cui X, Pan H-B, Wang S, Lin Y, Wai CM (2005) J Nanosci Nanotechnol 5:1852–1857
19. McCusker LB, Von Dreele RB, Cox DE, Louer D, Scardi P (1999) J Appl Crystallogr 32:36–50
20. Palosz B, Stelmakh S, Grzanka E, Gierlotka S, Palosz W (2007) Z Kristallogr 222:580–594
21. Plyasova LM, Molina IYu, Gavrilov AN, Cherepanova SV, Cherstiouk OV, Rudina NA, Savinova ER, Tsirlina GA (2006) Electrochim Acta 51:4477–4488
22. Langford JI, Louer D, Scardi P (2000) J Appl Crystallogr 33:964–974
23. Cherstiouk OV, Gavrilov AN, Plyasova LM, Molina IYu, Tsirlina GA, Savinova ER (2008) J Solid State Electrochem 12:497–509
24. Miller TM, Izumi AN, Shin Y-S, Whitesides GM (1988) J Am Chem Soc 110:3146–3156
25. An G, Yu P, Mao L, Sun Zh, Liu Zh, Miao Sh, Miao Zh, Ding K (2007) Carbon 45:536–542
26. Scardi P (2008) Microstructural properties: lattice defects and domain size effects. In: Dinnebeier RE, Billinge SJL (eds) Powder Diffraction: Theory and Practice. The Royal Society of Chemistry, Cambridge, pp 376–413
27. Scardi P, Leoni M (2002) Acta Crystallogr A58:190–200